

Fitting orbits to tidal streams

James Binney

Rudolf Peierls Centre for Theoretical Physics, Keble Road, Oxford OX1 3NP, UK

Draft, February 7, 2008

ABSTRACT

Recent years have seen the discovery of many tidal streams through the Galaxy. Relatively straightforward observations of a stream allow one to deduce three phase-space coordinates of an orbit. An algorithm is presented that reconstructs the missing phase-space coordinates from these data. The reconstruction starts from assumed values of the Galactic potential and a distance to one point on the orbit, but with noise-free data the condition that energy be conserved on the orbit enables one to reject incorrect assumptions. The performance of the algorithm is investigated when errors are added to the input data that are comparable to those in published data for the streams of Pal 5. It is found that the algorithm returns distances and proper motions that are accurate to of order one percent, and enables one to reject quite reasonable but incorrect trial potentials. In practical applications it will be important to minimize errors in the input data, and there is considerable scope for doing this.

Key words: stellar dynamics – methods: N-body simulations – Galaxy: kinematics and dynamics – Galaxy: structure

1 INTRODUCTION

Mapping the matter distribution in the outer reaches of the Galaxy, which is expected to be dark-matter dominated, is currently one of the central tasks in astrophysics. Recent surveys of the outer Galaxy have revealed numerous enhancements in the density of stars that have been securely identified as tidal streamers from Galactic satellites (Odenkirchen et al. 2001; Majewski et al. 2004; Belokurov et al. 2006). Such structures effectively delineate the orbit in the Galactic force-field of the parent body (Johnston et al. 1996; Odenkirchen et al. 2003). Knowledge of the phase-space coordinates along an individual orbit provides strong constraints on the force-field that confines the orbit, and thus on the matter distribution that gives rise to the force field. Consequently, in recent years considerable effort has been devoted to the problem of determining the orbit of a satellite from observations of its tidal stream (Law et al. 2005; Fellhauer et al. 2007).

Since tidal streams are generally discovered as enhancements in the density of stars on the sky, the phase-space coordinates of the satellite orbit that are easiest to determine are its Galactic coordinates $[l(u), b(u)]$, where u is an arbitrary parameter that increases along the orbit. With a moderate observational follow-up effort, it is always possible to augment these data with line-of-sight velocities $v_{\parallel}(u)$. The other three coordinates (heliocentric distance s and proper motion components) are much harder to obtain, and are generally either unknown or measured with very low accuracy.

Given the incomplete nature of the data, the standard approach to orbit fitting is to adopt a gravitational potential, and then to seek an orbit in this potential that is consistent with the data (e.g. Fellhauer et al. 2007). The fitting procedure is generally trial-and-error, and the final fit is often imperfect (e.g. Fellhauer et al. 2006).

Here we show that given the three coordinates (l, b, v_{\parallel}) along a section of an orbit in a gravitational potential $\Phi_0(\mathbf{r})$, one can uniquely determine what the remaining three phase-space coordinates must be if the data are to be part of an orbit in a trial potential $\Phi_t(\mathbf{r})$. If $\Phi_t = \Phi_0$, the recovered phase-space coordinates are consistent with conservation of energy, while when the trial and true potentials differ, energy conservation appears to be violated. Therefore this procedure can be used to hunt for the Galaxy’s gravitational potential, and yields predictions for distances and proper motions along a tidal stream that can be tested observationally.

2 THE ALGORITHM

We work in the inertial coordinate system in which the Galactic centre is at rest. Consequently, line-of-sight velocities in this frame will differ from measured heliocentric velocities by the projection of the Sun’s velocity (which we assume known) onto the line of sight. Let \mathbf{s} be the position vector of the satellite with respect to an observer at the position of the Sun, and let $\mathbf{F}_t(\mathbf{s})$ be the trial gravitational acceleration

arXiv:0802.1485v1 [astro-ph] 11 Feb 2008

($\mathbf{F}_t = -\nabla\Phi_t$). Then if the trial potential is correct, we have $\dot{\mathbf{s}} = \mathbf{F}_t$, and $v_{\parallel} = \dot{\mathbf{s}} \cdot \mathbf{v} = \dot{s}$ so $\dot{v}_{\parallel} = F_{\parallel} + \mathbf{v} \cdot d\hat{\mathbf{s}}/dt$, where F_{\parallel} is the component of \mathbf{F}_t along the line of sight. Also

$$\mathbf{v} = \frac{d(s\hat{\mathbf{s}})}{dt} = \dot{s}\hat{\mathbf{s}} + s\frac{d\hat{\mathbf{s}}}{dt} \quad (1)$$

so

$$\dot{v}_{\parallel} = F_{\parallel} + \frac{v^2 - v_{\parallel}^2}{s} = F_{\parallel} + \frac{v_{\perp}^2}{s}. \quad (2)$$

Moreover, the component of \mathbf{v} in the plane of the sky \mathbf{v}_{\perp} satisfies

$$|v_{\perp}|^2 = s^2\dot{u}^2 \equiv s^2(\dot{b}^2 + \cos^2 b \dot{l}^2), \quad (3)$$

where we have now fixed the meaning of the parameter u to be the angular distance along the trajectory. Eliminating $|v_{\perp}|^2$ between equations (2) and (3), we obtain a quadratic equation for dt that has solution

$$dt = \frac{1}{2F_{\parallel}} \left(dv_{\parallel} \pm \sqrt{dv_{\parallel}^2 - 4sF_{\parallel}du^2} \right). \quad (4)$$

Thus if we guess s at some point on the trajectory, we can solve for dt between observations, and calculate E . We get a new value of E for each pair of data points. We can also update s from $ds = v_{\parallel}dt$.

To obtain a robust numerical scheme we divide $ds = v_{\parallel}dt$ and equation (4) by the differential of u to obtain the set of coupled ordinary differential equations

$$\begin{aligned} \frac{dt}{du} &= \frac{1}{2F_{\parallel}} \left(\frac{dv_{\parallel}}{du} \pm \sqrt{\left(\frac{dv_{\parallel}}{du}\right)^2 - 4sF_{\parallel}} \right) \\ \frac{ds}{du} &= v_{\parallel} \frac{dt}{du}. \end{aligned} \quad (5)$$

The sign ambiguity in the first equation is resolved such that t increases along the trajectory.

3 TESTS

The algorithm was tested by reconstructing orbits from pseudodata obtained by projecting orbits in a model potential. The tests showed that it is important to determine accurately the distance u along the trajectory to each data point. This can be determined in a two-step process: we first obtain a crude estimate

$$\lambda_i = \sum_{j < i} \sqrt{(b_{j+1} - b_j)^2 + \cos^2[\frac{1}{2}(b_{j+1} + b_j)](l_{j+1} - l_j)^2}. \quad (6)$$

Then we fit cubic splines in λ to the values $b_i = b(\lambda_i)$ and $l_i = l(\lambda_i)$, and use the resulting functions of λ to evaluate numerically the integrals

$$u_i = \int_0^{\lambda_i} d\lambda \sqrt{b'^2 + \cos^2(b)l'^2}, \quad (7)$$

where a prime denotes differentiation with respect to lambda. Finally we fit cubic splines to the values $b_i = b(u_i)$, etc., and use these functions of u and the fourth-order Runge-Kutta algorithm to solve equations (5). At each integration step we re-evaluate $E = \frac{1}{2}(v_{\parallel}^2 + s^2\dot{u}^2) + \Phi_t$.

Orbits were integrated in the Miyamoto–Nagai potential that has $b/a = 0.2$ and $GM/a = 1$ (Miyamoto & Nagai

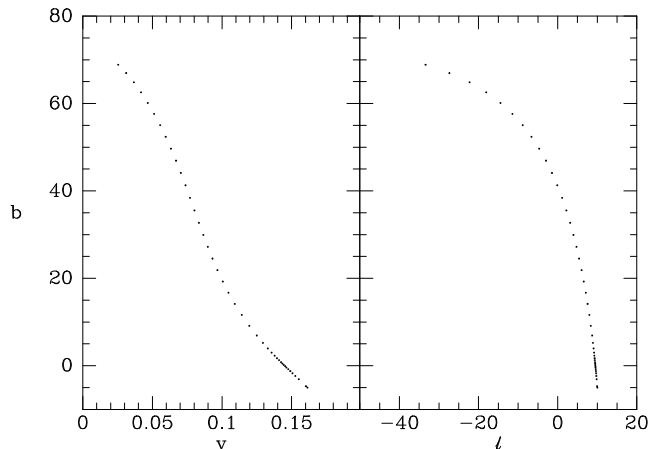


Figure 1. Right panel: the projection onto the sky of a numerically integrated orbit in a Miyamoto–Nagai potential with $b/a = 0.2$. Left panel: the line-of-sight velocity as a function of b .

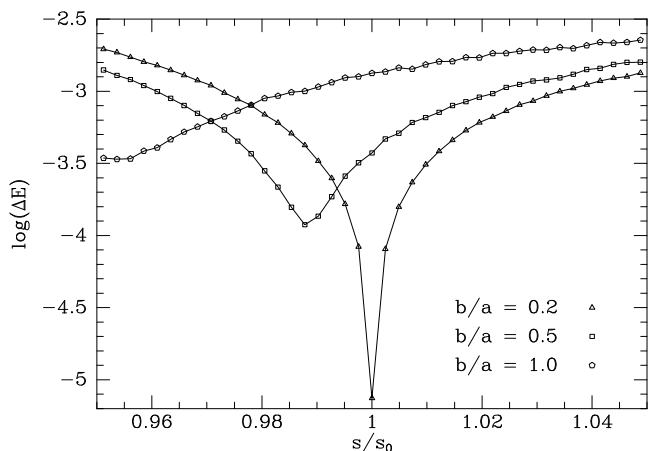


Figure 2. The log to base 10 of the rms variation in the energy when the orbit shown in Fig. 1 is reconstructed from an assumed initial distance s rather than its true value s_0 . The triangles show results obtained when the reconstruction employs true potential, while the squares and pentagons are for less flattened potentials.

1975, and Fig. 4). They were then reconstructed using either this potential or a Miyamoto–Nagai potential with different parameters. The 42 dots in the right panel of Fig. 1 show the input coordinates on the sky of the model orbit when it is viewed from a point in the symmetry plane and $8a$ from the centre, while the left panel shows the line-of-sight velocities along the orbit. The orbit has energy $-0.0322GM/a$. It starts at $b = -5$ deg and a distance $15a$ from the point of observation, and moves out to a distance $22.6a$ as it rises to $b = 68.9$ deg. The triangles in Fig. 2 show the rms variation ΔE in the output energy E along the reconstructed orbit when the true potential is used to integrate equations (5) from these data points and an initial distance s that is the stated multiple of its true value, s_0 . There is a sharp minimum in ΔE when $s = s_0$. The squares and pentagons in Fig. 2 show the corresponding results when the wrong potential is used to reconstruct the orbit – larger values of b/a generate rounder potentials.

When the potential is correct, we find to a good approximation that $\Delta E \propto |1 - s/s_0|$, while with an incorrect

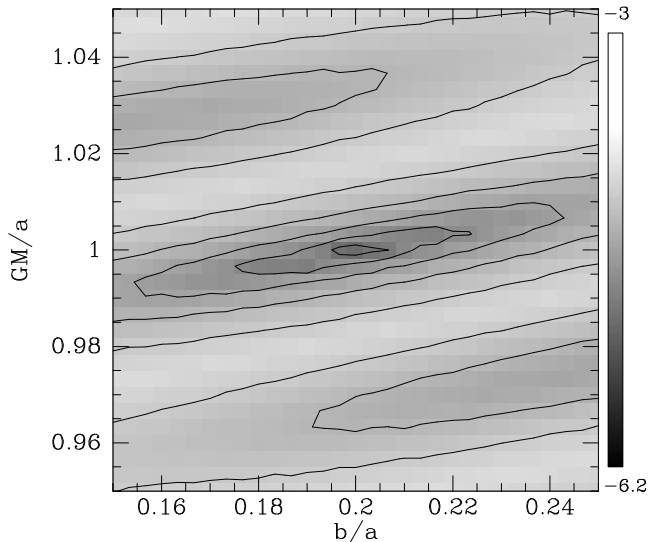


Figure 3. A contour plot of $\log_{10}(\Delta E)$ as a function of the parameters used in the reconstruction of the orbit segment shown in Fig. 1.

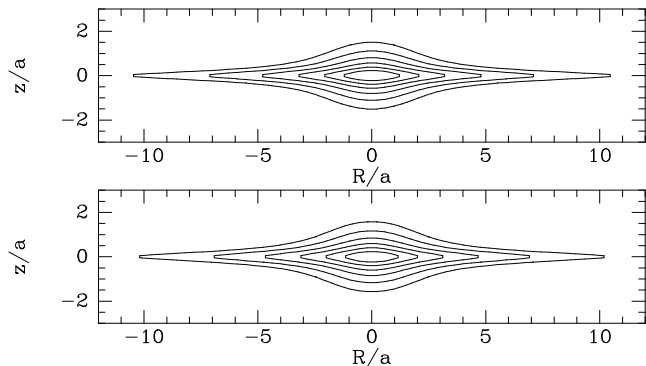


Figure 4. Isodensity contours in the meridional planes of Miyamoto–Nagai models with $b/a = 0.2$ (top) and $b/a = 0.22$ (bottom).

potential the curve of ΔE can be fitted near its minimum with $\Delta E \propto \sqrt{(1 - s/s_0)^2 + k^2}$ with $k \neq 0$. Thus in a practical case the quantity k can be used as a measure of how far the potential employed differs from its true value.

Fig. 3 explores the effect of varying both the parameters b/a and GM/a of the potential used in the reconstruction of this orbit. Although an error in one parameter can to some extent be offset by an error in the other parameter, there is a sharp minimum in ΔE when the parameters take their true values. Thus from this one orbit one can determine both the flattening and the mass of the potential with precision. Fig. 4 illustrates how high this precision is by showing isodensity contours of the Miyamoto–Nagai models that have $b/a = 0.2$ (top) and 0.22 . Although these models are extremely similar, analysis of the orbit segment easily distinguishes them.

Changing the length of the orbit segment analysed by a factor 3 either side of the length shown in Fig. 1 does not change the results significantly. In particular, the algorithm identifies incorrect potentials even with quite short orbit segments.

These tests demonstrate that with high-quality data the algorithm has no difficulty recovering the true orbit if the potential is the correct one, and provides excellent discrimination against incorrect potentials.

3.1 Multiple orbit segments

Different streams will be sensitive to different aspects of the Galactic potential – streams near the plane will be sensitive to the structure of the disc, while the Magellanic Stream must be insensitive to the disc but sensitive to the total Galactic mass. The Galactic potential would be most strongly constrained by a plot like that shown in Fig. 3 in which the quantity contoured is the sum of ΔE for all available streams.

Obscuration by dust near the plane sometimes breaks a stream into two or more segments with an unobserved gap between them. In principle each segment could be analysed independently, but this would not be the optimal procedure. First, all segments should be used to determine the path of the underlying orbit on the sky, including through obscured regions. Then the algorithm should be used to reconstruct each segment, and the rms energy variation along all reconstructed segments (treated as a whole) minimized within the space spanned by the initial distances assumed for each section.

3.2 Effect of errors in the data

In practice the input data will be less exact than in the tests above because tidal streams have finite widths on the sky and do not exactly trace a single orbit. In favourable cases they delineate an orbit with great precision: for example the tidal stream of a globular cluster such as that of Pal 5 is precisely bounded by the cluster’s orbit (Odenkirchen et al. 2003). The tidal streams of larger bodies, such as the Sgr dwarf galaxy, are broad, and their relation to the orbit of the progenitor is less evident. Correspondingly, in the case of a globular cluster, the uncertainty in the radial velocity along the stream will be limited to measurement errors in the velocities of stars, while in the case of a dwarf galaxy one has to contend also with the velocity dispersion of the progenitor, which both widens the range of velocities encountered at any point on the stream and leads to a systematic offset between the mean velocity in the stream and the velocity of the underlying orbit.

When applying the algorithm to a stream such as that of Pal 5, one would not use the positions and velocities of individual stars directly but would make a judgment as to the relation of the orbit to the stellar stream, and estimate the radial velocity on the orbit by averaging the velocities of nearby stars and then making a correction for the expected offset between the stream and orbital velocities. When all this had been done, one would contrive that the trajectory of the orbit on the sky and in radial velocity was smooth. Therefore, in tests it is not appropriate to add independent errors to each data point, but rather to add correlated errors that leave the trajectory through (l, b, v_{\parallel}) space smooth. We do this as follows. For $x = v_{\parallel}, b, l \cos b$, we add a Fourier series

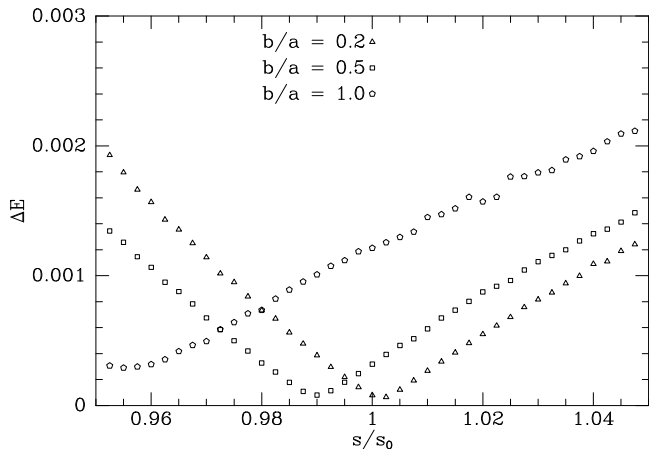


Figure 5. As for Fig. 2 except that equation (8) has been used to add errors to b and $l \cos(b)$ that each amount to 2 arcmin rms. The minimum value of ΔE for $b/a = 0.5$ is bigger than for $b/a = 0.2$ by a factor 1.3.

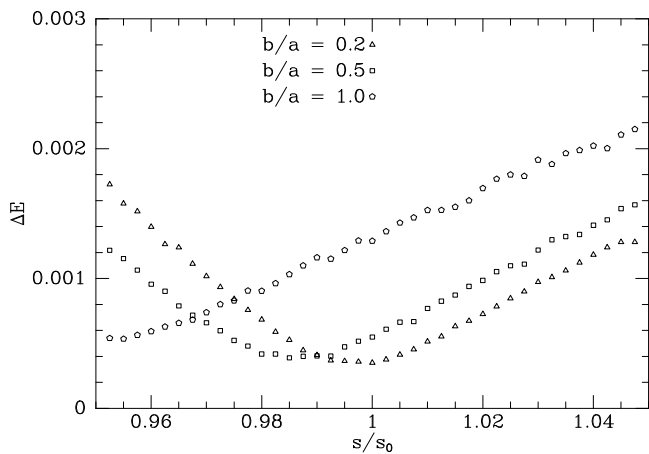


Figure 6. As for Fig. 2 except that equation (8) has been used to add errors to v_{\parallel} that amount to 0.1 percent of the circular speed at the start of the segment. The minimum value of ΔE for $b/a = 0.5$ is bigger than for $b/a = 0.2$ by a factor 1.1.

$$\delta x(u) = \sum_n X_n \cos(2n\pi\hat{u} + \xi_n), \quad (8)$$

where $n = 0-9$ is an integer, $\hat{u} = u/u_{\max}$ ranges from zero to unity along the trajectory, and ξ_n is randomly distributed in $(0, 2\pi)$. The amplitudes X_n determine the power spectrum of the noise. We have no way of knowing what this would be, but have assumed that $X_n \propto (1+n)^{-1.1}$.

Studies of the tidal stream of Pal 5 provide a guide to the magnitude of the errors to be encountered in real data. The stream's full width is ~ 30 arcmin (Odenkirchen et al. 2003), so it should be possible to determine the position of the underlying orbit with an error that does not exceed a tenth of this, and could be substantially smaller. Odenkirchen et al. (2002) report velocities along the stream that have errors $\sim 0.15 \text{ km s}^{-1}$ plus a dispersion of order 0.9 km s^{-1} arising from binarity. The latter dispersion could be beaten down by making observations at several epochs; even at one epoch, measurements of many stars would enable the velocity of the underlying orbit to be obtained to

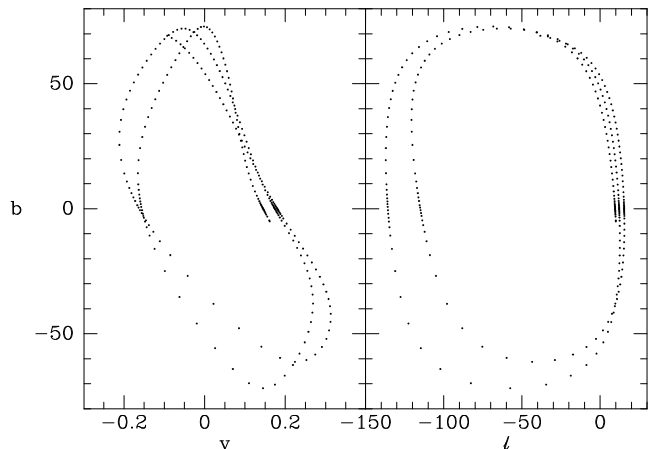


Figure 7. Data points for an orbit segment ten times as long as in Fig. 1.

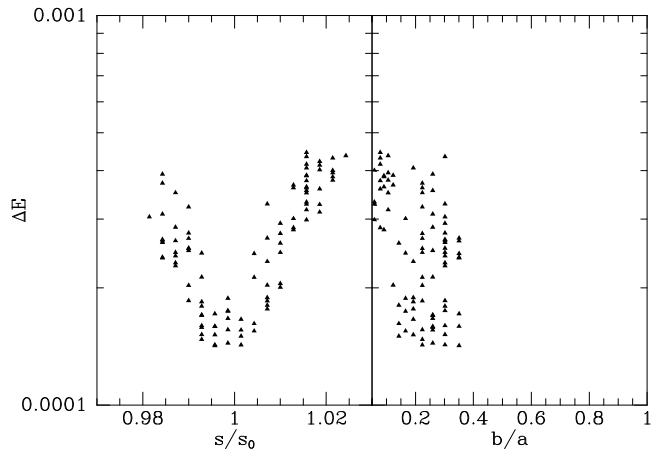


Figure 8. The results of reconstructing 100 realizations of the orbit segment of Fig. 7, with astrometric errors of 2 arcmin and velocity errors of 0.1 percent of v_c . The points show the values of s/s_0 and b/a that gave the smallest value of ΔE , together with that value of ΔE .

a precision of at least 0.2 km s^{-1} . Hence we focus here on errors of 2 arcmin in b and $l \cos(b)$, and errors in v_{\parallel} that are 0.1 percent of the circular speed at the start of the orbit segment.

Fig. 5 shows that with these errors in b and $l \cos(b)$ it is still possible to determine the distance to the orbit with exquisite accuracy, and to tell that the potential with $b/a = 0.2$ is to be preferred to that with $b/a = 0.5$.

Fig. 6 shows the results obtained when the radial velocities are in error by 0.1 percent of the circular speed at the starting point of the segment. The impact of these velocity errors is larger than that of the position errors. However, it is still just possible to reject the potential with $b/a = 0.5$, and the distance is accurately determined even if the wrong potential is chosen. When the orbit segment used for the reconstructions covers a time interval that is longer by a factor ten (Fig. 7), it becomes possible to reject the potential with $b/a = 0.5$ with security. Fig. 8 illustrates this finding by showing for each of 100 different realizations of the noise added to the positions and velocities of Fig. 7 the best fitting values of s/s_0 and b/a together with the associated

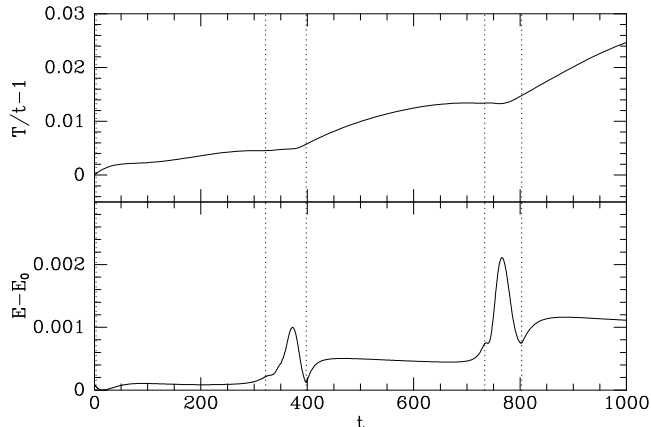


Figure 9. Variation in reconstructed energy E and time T along the orbit shown in Fig. 7 when the correct potential and distance are used when v_{\parallel} is in error by 0.1 percent of v_c . The vertical dotted lines mark the times when the orbit passes through the plane.

values of ΔE . All distance estimates lie within 2 percent of the truth; the mean of $s/s_0 = 1.002$ while its rms dispersion is 0.012. Values of b/a in the range (0.1, 1) were searched but no value bigger than 0.35 was recovered; the mean of $b/a = 0.201$ while its rms dispersion was 0.095. Thus with these errors in the data it is possible to say that the potential is highly flattened, but not actually determine b/a .

Fig. 9 shows the reconstructed values of time and energy along the best reconstruction of the long segment plotted in Fig. 7 when the velocities are in error by 0.1 percent of the circular speed. Vertical dotted lines mark the instants at which the orbit passes through the plane; pericentre and the point of closest approach to the Sun lie between pairs of these plane-crossings. Some combination of plane crossing and the peak in the proper motion as the orbit passes closest to the Sun induces features in both the time and energy plots. These features are independent of the accuracy parameter specified for the integration of equations (5), and they have no analogues when error-free data are used for the reconstruction. The reconstructed time T is systematically later than it should be by a few percent, and the reconstructed energy is correspondingly larger than it should be.

Since the proper motions that the algorithm predicts are inversely proportional to the elapse of T along the stream, the figure shows that even with errors in the input velocities, proper motions are generally accurate to a few percent.

The algorithm's sensitivity to errors in v_{\parallel} arises because the underlying physical idea is that the change in v_{\parallel} between data points requires a certain time interval, and this time interval determines both the change in distance between the points and the orbit's proper motion. Thus the reconstruction is driven by differences in v_{\parallel} , which are sensitive to errors in v_{\parallel} . When equation (8) is used to simulate errors, the error in the difference in v_{\parallel} between neighbouring points scales like u_{\max}^{-1} , so longer orbit segments produce more accurate results.

4 CONCLUSIONS

A tidal stream delineates the orbit of its progenitor, so it can be used to obtain three phase-space coordinates of an orbit. To complete the specification of the orbit, one needs to associate with each of its points on the sky a distance and a time of passage. The algorithm presented here yields these additional quantities for an assumed potential and a distance to one point on the stream. Unless these two inputs are correct, there is no guarantee that energy will be conserved along the reconstructed orbit, and indeed numerical experiments show that with noise-free data, the rms variation in energy along the reconstructed orbit allows one to identify the potential and determine the correct initial distance.

The algorithm is less sensitive to realistic errors in the position of the stream on the sky than to likely errors in v_{\parallel} because the reconstruction is driven by *differences* in v_{\parallel} between grid points.

The algorithm predicts the distances and proper motions of objects in the stream, so when these data are available, they will provide an interesting check on the correctness of all inputs and assumptions. Crude distance estimates are generally available and seriously erroneous potentials can probably be excluded because they return astrophysically unacceptable distances. With presently attainable accuracy of the input data it should be possible to determine distances to within about one percent, and to constrain the Galactic potential quite strongly.

It is important to recognize that the inputs to the algorithm should be the sky coordinates and line-of-sight velocities of the orbit of a test particle, not the corresponding coordinates of a stream; streams delineate orbits, but they do not actually lie along them. In practice a significant effort will be required to extract the optimum input data from measurements of any given stream, and an optimal approach to this task does not appear to have been published. However, the experiments presented here indicate that the rewards for obtaining accurate input data will be very high: even one orbit segment provides a wealth of precision information about the Galactic potential and observationally testable predictions about the stream. The Galactic potential could be even more strongly constrained by analyzing several orbit segments together.

ACKNOWLEDGMENTS

It is a pleasure to thank Andy Eyre, John Magorrian and the referee, Konrad Kuijken, for valuable suggestions.

REFERENCES

- Belokurov, V., et al., (15 authors) 2006, ApJ, 642, L137
- Fellhauer M., et al., (12 authors) 2006, ApJ, 651, 167
- Fellhauer M., Evans N.W., Belokurov, V., Wilkinson M.I., Gilmore G., 2007, MNRAS, 380, 749
- Johnston K.V., Hernquist L., Bolte M., 1996, ApJ, 465, 278
- Majewski S.R., et al. 2004, AJ, 128, 245
- Miyamoto M., Nagai R., 1975, PASJ, 27, 533
- Odenkirchen M., et al., 2001, ApJ, 548, L165

Odenkirchen M., Grebel E.V., Dehnen W., Rix H.-W.,
Cudworth K.M., 2002, *AJ*, 124, 1497

Odenkirchen M., et al., (10 authors) 2003, *AJ*, 126, 2385

Law D.R., Johnston K.V., Majewski S.R., 2005, *MNRAS*,
619, 807